11 igh Current Cathode Thermal 1 Behavior, Part II: '1 heory

K. D. Goodfellow* and J. E. Polk*
Jet Propulsion Laboratory
California Institute of Technology
Pasadena, California

Abstract

Cathode erosion is one of the life limiting mechanisms for several classes of electric thrusters. Since cathode erosion is strongly dependent on the cathode temperature, a quantitative understanding of the effects of cathode operation on the cathode temperature is required. The development of a cathode/plasma interaction model for determining the heat loads to the cathode as functions of the various free stream plasma parameters is presented. This model is combined with a cathode thermal model in order to provide a complete and integrated picture of high current cathode operation. Several computational examples are used to illustrate the combined model.

Introduction

One of the major issues for the use of electric propulsion thrusters is lifetime. Missions analyses estimate that for electric propulsion to be a viable option, thruster lifetimes must be of the order of 1000 to 15,000 hours. Cathode erosion, one of the primary life-limiting mechanisms, has been shown to depend strongly on the cathode temperature [1]. Therefore, part of this study is intended to provide a simple means of predicting the cathode temperature for various thruster operating conditions. In addition, the thermal characteristics of the electrodes must be known to compute the overall thruster thermal loads to the spacecraft. This model also provides the appropriate boundary conditions at the cathode surface for models of the operating characteristics of the thruster. For example, the current contours within the magnetoplasmadynamic (MPD) thruster cannot be specified independently of the cathode temperature distribution because the majority of the current is from thermionic emission. Since the cathode model boundary conditions also depend on the characteristics of the main plasma, the two models must be ultimately coupled to obtain an overall model of the cathode region of the thruster.

Several different approaches have been taken in the past to characterize the nature of the hot-cathode arc physics. Typically two models are considered, one describing the plasma near the cathode and the other modeling of the thermal characteristics of the cathode. Past works have focussed primarily on one or the other of these models, but both are needed since they are closely coupled. That is, the plasma model provides the heat loads (boundary conditions) for the thermal model, and the thermal model provides the surface temperature which strongly affects the plasma near the cathode through thermionic emission.

Additionally, an elementary approach to an overall model is to consider an energy balance for the MPD thruster[2]. The difficulty with this approach is in determining the heat loads to the electrodes which are typically approximated as a simple fraction of the electrical input power. That is, for a thruster operating at 100 kW of electrical power, 40 percent (or 40 kW) may be lost as anode heating and 20 percent (or 20 kW) may be lost as cathode heating. This approach can be useful for examining experimental data. Shih et al. [3] used calorimetry on the anode, cathode and plume to determine the energy distribution within the MPD thruster. They then, using the input current, determined "equivalent voltage drops"

*Member of the Technical Staff, Member AIAA

for the anode and cathode. That is, thermal characteristics were used to help describe the discharge characteristics.

A simple model of cathode sheath was developed by Prewett and Allen to describe the double sheath associated with a thermionically emitting cathode [4]. This model has been previously used to describe arcjet [5] and MPD thruster cathode heating [6]. The model developed by Siegfried and Wilbur [7] combines this sheath model [4] with an ionization zone, surface current and energy balances, and empirical relations for the flow field within the hollow cathode. A similar model is presented by Salhi and Turchi [8], except that the empirical model is replaced with an isothermal flow model.

Compared to the plasma, a thermal model of the cathode is generally straight-forward but may be numerically challenging. Simple one and one-half dimensional (axial temperature distribution with radial heat inputs) models have been presented by Bade and Yos[9] and Mehta[10]. Mehta's model includes radial convection and radiation, Ohmic heating, and constant material properties (temperature independent) for specified tip and base temperatures. Note that neither of these models are capable of including radial heat loads from arc attachment. The model by Weng and Seldin [11] considers the axial and radial temperature distributions within the cathode of an electric steel furnace. While the thermal model may seem simple, numerical difficulties arise from the nonlinearities, specifically, temperature dependent material properties, radiation, and arc heating.

Two simple models have been developed for the combined (plasma-cathode heating) solution. Bade and Yos[9] developed a model which combines a simplified sheath model with a simple thermal model for arcjet cathodes (arc attachment at the tip only). The model presented by King [12] for an MPD thruster includes a simplified sheath model (neglecting the plasma electron contribution) with a surface energy balance. While this model is appropriate for high cathode voltages, neglecting the plasma electron contribution can significantly affect the results for low voltages ($\lesssim$ 10 volts) which are more appropriate for steady-state MPD thrusters.

Cathode Model

The cathode model consists of two parts, namely a near-cathode plasma model and a thermal model of the cathode. The near-cathode plasma model connects the properties of the main plasma with the cathode. Specifically, given the plasma properties within a mean-free-path of the surface, the near-cathode model predicts the heat flux and current density to the cathode surface. With these boundary conditions and the traditional thermal transport mechanisms, the thermal model can predict the temperature distribution within the cathode. Because of the interdependency of the two models, they must be solved simultaneously.

Near-Cathode Plasma Model

An illustration of the near-cathode plasma is shown in Fig. (1). The Debye length, mean free path,

Figure 1: Near-cathode plasma regions.

and thermal, concentration and momentum boundary layers are represented by l_D, l_{ei} and $l_{T,C,M}$ respectively. For this study, only the surface, sheath, presheath and ionization regions are modeled. The relative magnitudes of the ion and plasma electron currents differ in each of the near-cathode regions. In the main body of the plasma, the current is predominantly carried by the electrons, while in the sheath region the ion current may dominate. To match these regions an ionization region (which produces the required number of ions for the sheath region)

is required between the sheath and the main plasma body. Similarly, a recombination region exists at the cathode surface to produce a transition to pure electron conduction in the solid. At the surface, ions are also converted to neutrals, which then return to the plasma. Each of the regions will be briefly discussed in the following sections. A complete description of each region model, the overall near-cathode plasma model and sample solutions are given in Ref. [13].

Cathode Surface/Recombination Region

In general the cathode surface is characterized by the material, the surface finish and the temperature. For this model, the recombination region is assumed to be infinitesimally thin and is considered as a surface effect. Incident particles from the sheath heat the surface while emitted particles cool the surface. The energy balance at the surface balances the energy deposited and removed by the particles with heat conduction into the solid, and radiative, convective and mass (surface erosion) transport to the surroundings. The net heat flux to the surface due to the plasma is given by

$$\begin{aligned} q_{tot} &= q_i + q_e - q_b - q_n \\ &= j_i\,(eV_c + eV_R + \epsilon_i - \phi_{eff}) \\ &\quad + j_e\left[\phi_{eff} + 2kT_e\left(1 + \frac{eV_c}{2kT_e}\right)\right] \\ &\quad - j_b\left(\phi_{eff} + \frac{2kT_c}{e}\right) - F_{n,c}\,2kT_c \end{aligned} \tag{1}$$

and the net current is given by

$$j_{tot} = j_i + j_b - j_e. \tag{2}$$

The first major term in Eq. (1) represents the energy from the ions, the second term from the plasma electrons, the third term from the thermionic electrons, and the fourth is the thermal energy removed by the neutrals. In the ion term, the subterms represent the energy gained from the voltage drop through the sheath and presheath regions plus the energy resulting from the recombination of the ions at the surface. The plasma electron term contains the energy for condensation of an electron on the material plus the thermal energy of the electrons. Note that this thermal energy contains two terms because only the tail electrons of the Boltzmann distribution are considered. The retarding sheath potential serves to reject plasma electrons with insufficient kinetic energy. The energy flux to the surface is therefore obtained by integrating over the population of electrons that have sufficient energy to overcome the sheath potential, resulting in the two terms shown in Eq. (1) for the plasma electron thermal energy. The thermionic electron term consists of the energy required by an emitted electron to escape from the surface work function barrier plus its thermal energy. The surface is assumed sufficiently rough to be fully accommodating so that the emitted neutral flux is equal to the ion current ($j_i = eF_{n,c}$). The emitted particles are assumed to be Maxwellian with energies proportional to the surface temperature. While the terms representing the thermal energy removed by the thermionic electrons and the neutrals are small compared to the other terms, they are not negligible and can be of the order of tens of percent of the other terms under certain conditions, such as low sheath voltages or for gases with low ionization potentials such as lithium. In addition, radiative and convective transport from the surface as well as conduction into the material are also considered for the overall energy balance, depending on the specific problem. These effects are included in the thermal model.

For high cathode temperatures, thermionic emission is the dominant current conduction mechanism in the near-cathode region [12]. Thermionic emission is described by the empirical Richardson-Dushman relation shown in Eq. (3). The thermionic emission is extremely sensitive to the values of the Richardson coefficient, A_R, and the material work function ϕ. A 1/2 eV change in work function can produce more than an order of magnitude change in current density. The Richardson coefficient and the work function may also be temperature dependent. Past authors usually model one of these parameters as a function of the surface temperature while the other remains constant[14]. In addition, the surface electric field acts to enhance the emission, a phenomenon known as the Schottky effect [15]. The effect is shown as a lowering of the material work function in Eq. (4),

$$j_b = A_R T_c^2 \exp\left(-\frac{\phi_{eff}}{kT_c}\right) \tag{3}$$

$$\phi_{eff} = \phi_o - \sqrt{\frac{eE_c}{4\pi\epsilon_o}} \tag{4}$$

The magnitude of the electric field at the cathode surface is primarily determined by the characteristics of the sheath region. The Schottky effect can significantly change the thermionic emission current density. For the conditions of interest in this study, the Schottky effect may change the work function by several tenths of an electron volt, resulting in significant changes in the thermionic current.

Sheath Region

The sheath region is assumed to contain collisionless particles with constant total energy (potential plus kinetic). Three species are considered, namely monoenergetic thermionic (or beam) electrons, singly charged monoenergetic ions, and Maxwellian electrons originating in the plasma [4] [6]. Further, the sheath thickness is assumed to be much less than the Larmor radii of the particles, and therefore, magnetic fields affect the particle trajectories are negligible.

The model developed here is similar to the one presented in Ref. [4] but also includes the thermal energy of the thermionic electrons, E_{bo} $(= 2T_e/T_e)$, and uses a normalization such that the normalized thermionic current density, J_b, is independent of the normalized sheath voltage, η_e. For a stable sheath to occur, the ions must enter the sheath with energies equal to or greater than the Bohm minimum energy [16]. The ions here are assumed to enter the sheath with energies equal to the Bohm minimum energy which is represented as the Bohm potential, V_B. The plasma electrons are assumed to be Maxwellian and referenced to the electron density at the sheath edge. These electrons fall into two classes, namely those with sufficient kinetic energy to overcome the sheath retarding potential and reach the cathode surface and those with insufficient energy that are repelled back to the main plasma. The corresponding flux of the high energy electrons constitutes the plasma electron current. The one-dimensional Poisson charge equation is used to describe the electric field and the electric potential

The voltage at the sheath edge was set to zero as a reference point and the electric field is assumed to be ϵ_{sh} at the sheath edge. The sheath region model provides a relation for the electric. field at the cathode surface given by Eq. (5). This equation is used to compute the Schottky effect and completes the description of the thermionic emission current given in Eq. (3) and Eq. (4).

$$\epsilon_c^2 = \left(\frac{eE_cL_D}{kT_e}\right)^2 = 4\nu_i\eta_B\left[\left(1 + \frac{\eta_e}{\eta_B}\right)^{1/2} - 1\right] - 4J_b\left[(\eta_e + E_{bo})^{1/2} - E_{bo}^{1/2}\right] + 2e^{-\eta_e} - 2 + \epsilon_{sh}^2 \quad (5)$$

Expressions for the normalized ion number density and the normalized Bohm energy are given in Eq. (6) and Eq. (7) respectively.

$$\nu_i = \frac{n_{i,o}}{n_{e,o}} = 1 + J_b(\eta_e + E_{bo})^{-1/2} \quad (6)$$

$$\eta_B = \frac{eV_B}{kT_e} = \frac{\nu_i}{2 - J_b(\eta_e + E_{bo})^{-3/2}} \quad (7)$$

Presheath and Ionization Regions

The ionization and presheath regions connect the sheath region with the main plasma body [9] [15]. The purpose of the presheath region is to accelerate the ions so that they enter the sheath region with the minimum energy required for a stable sheath (Bohm energy) [1 G]. For this model the presheath region is combined with the ionization zone by requiring that ions leave the ionization region with the Bohm energy. The ionization region generates the required number of ion and electron pairs to match the sheath and main plasma body values. An illustration of the particles entering and leaving the ionization region is shown in Fig. (2). The number density of the electron and ion pairs that can be produced by ionization is determined by the energy balance. Since only singly charged ions are considered, the production rates of the ions, n_i, and the electrons, n_e, are equal. Since the cathode surface is assumed to be fully accommodating, the ion flux, j_i/e, to the sheath and the flux of neutrals from the surface, $F_{n,c}$, are equal. The energy equation in the ionization region can be written as

$$j_b[e(V_c + V_B) + 2kT_e] - j_i(eV_B + \epsilon_i - 2kT_e) - j_e 2kT_e\left[1 + \frac{e(V_c + V_B)}{2kT_e}\right] - j_{tot}\left(2kT_e - \frac{m_e}{m_i}\epsilon_i\right) = 0. \quad (8)$$

Figure 2: Illustration of ionizat ion region.

The predominant terms are the energy added to the region by the thermionic electrons, the energy consumed by ionization, the energy removed by the ions to the sheath, and the energy removed by the plasma electrons to both the sheath (third term) and the main plasma (fourth term). The relative sizes of the current densities determine which energy removal term dominates. The energy equation can be normalized into a trancendental equation of three variables, η_c, J_b and E_{bo} [13].

Previous authors have used a simpler form of Eq. (8),

$$j_b V_c = j_i \epsilon_i. \tag{9}$$

That is, all of the energy gained by the thermionic electrons in the sheath is used to create ions [9] [15]. This equation provides an algebraic relation between the sheath voltage and the thermionic current as compared to Eq. (8) which is transcendental. Note that although Eq. (8) is more complicated than Eq. (9) it does not contain any new variables (including the sheath region).

Neumann considered argon and helium at 1 atm [15]. A semi-infinite thoriated tungsten cathode ($\phi = 2.6$ eV, $A_{II} = 1$ A/cm^2/K^2), with current densities of 3536 to 3837 A/cm^2 with sheath voltages of 31.09 and 4.66 volts, respectively, was analyzed. For this range, the plasma electron current ranges from negligible at 31.09 volts to 30 percent of the total current at 4.66 volts, and the products in Eq. (9) range from 37.6 to 17.8 kW/cm^2 respectively. Clearly, the plasma electron current cannot be neglected for low-voltage situations.

There are upper and lower limits on the number of ion/electron pairs in the ionization region. The upper limit on the number of possible ions produced is set by the pressure assuming fully ionized plasma ($\alpha = 1$), given in

$$n_{i,max} = \frac{P}{2kT_e} \tag{10}$$

If this limit is reached, the excess energy to the ionization region is assumed to be dissipated in modes other than ionization or thermal energy. Similarly, if the plasma is sufficiently ionized already, then a minimum number of ions exist as shown in

$$n_{i,min} = \frac{P}{kT_e} \frac{\alpha}{1+\alpha} \tag{11}$$

That is, ion/electron pairs produced outside of the ionization region are used. The ionization fraction represents the number of ions per heavy particle (ions plus neutrals). The values for the pressure and the ionization fraction only affect these limiting conditions and have no effect if the number of ions produced is governed by the energy balance. In other words, if the number density calculated by the energy balance is lower than the minimum value set by the ionization fraction then the value set by the ionization fraction is used. Similarly, if the number density value from the energy balance is greater than the value set by the pressure, the value calculated from the pressure is used.

There are many other effects that have been neglected in this formulation, for example, radiation to/from both the main discharge and the surface, and nonequilibrium effects. Also, the ions within an MPD thruster can achieve axial velocities greater than 50 km/s which may significantly change the ionization characteristics along the cathode from the base to the tip.

Overall Near-Cathode Plasma Model

The surface, sheath and presheath/ionization region models are combined to form the overall near-cathode plasma model. The heat flux and the current

density to the surface are determined for values of the electron temperature, T_e, the cathode temperature, T_c, the sheath voltage, V_c, the pressure, P, the ionization fraction, α, the surface material, and the gas type. While the normalized parameters are useful for examining the characteristics of each region, they are not useful for the combined model. This is because the term in the empirical relation for the thermionic emission current (Richardson-Dushman equation) for the Schottky effect does not normalize in the same manner as the other equations. Therefore the computations were performed using the unnormalized variables.

The relative values of the ion and plasma electron current are predominantly determined by the sheath voltage. The heat flux to the cathode surface increases until the maximum ion number density, which is set by the pressure in the ionization region, is reached, and then decreases. For cathode temperatures below the peak, ion and plasma electron heating dominate, while for values above the peak the ion and plasma electron heat fluxes are approximately constant. (A slight increase in the ion heat flux occurs because the Bohm energy is weakly dependent on the cathode temperature.) Therefore, the total heat flux decreases because the thermionic electron cooling effect begins to dominate. It is this set of curves that forms the boundary conditions for the thermal model. The near-cathode plasma model is most sensitive to the material work function as expected due to the exponential nature of the Richardson-Dushman equation.

Thermal Model

For a given set of boundary conditions, the thermal model describes the temperature distribution within the cathode. There are several orders of approximation by which the thermal model can be done ranging from simple one-dimensional analytical models to complex two dimensional (axisymmetric) numerical ones. The nonlinearities of the near-cathode plasma model can cause numerical difficulties for the thermal model. The heat flux to the surface from the plasma model is sensitive to the surface temperature. The thermal model must be resilient enough to handle large boundary condition changes during the numerical iterations. While the simple models do not have the capabilities for solving the problems of interest, they provide useful insights into the solution trends and provide good first approximations for the starting conditions for the more advanced models.

One-Dimensional Models

The simplest thermal model is one-dimensional heat conduction, given by

$$q = \frac{A_C k_{th}}{L} (T_{tip} - T_{base}) \qquad (12)$$

A slightly more advanced thermal model includes radial external heat removal where the cathode is assumed to be uniformly cooled by convection (or linearized radiation). These models are often referred to as one and one-half dimensional models. A cathode with a large length to diameter ratio, L/d, can be effectively modeled as an "infinite fin" with a heat flux given by Eq. (13) and the axial temperature distribution by Eq. (14) [17].

$$q = \sqrt{\frac{h_{conv} k_{th} \pi^2 d^3}{4}} (T_{tip} - T_\infty) \qquad (13)$$

$$T = (T_{base} - T_\infty) \exp\left(-\sqrt{\frac{4h_{conv}}{k_{th} d}} z\right) + T_{base} \qquad (14)$$

For cathodes with smaller L/d ratios it is more appropriate to specify either the base temperature or the heat flux from the base. These models are more appropriate for cathodes with water cooling at their base, such as the cathode in the Stuttgart ZT1 thruster or the JPL cathode test facility (CTF) [18]. Solutions for other electrode base conditions can also be found in Ref. [17]. While this model adds radial heat removal, it is restricted to one value for the heat transfer coefficient, h_{conv}. For an actual thruster, the heat transfer coefficient may vary significantly along the length of the cathode. These models provide a good first approximation for arcs with only tip attachment, such as arcjets.

For an accurate thermal model of the MPD thruster cathode, the ohmic heating must be included. Calculations for the large currents required in MPD thrusters show that ohmic heating is the dominant electrode heating mechanism. For example, a 12111111 diameter tungsten cathode 65 mm long produces 1.4 kW by ohmic heating at 2000 A ($\rho_e = 60 \times 10^{-8}$ Ω-m).

A one and one-half dimensional numerical solution for a cathode which includes radial radiation and convection, and ohmic heating, for a cylindrical rod with a conical tip is presented in Ref. [10] for the steady-state case and in Ref. [19] for the transient case. This model assumes constant properties (convection coefficient, emissivity, thermal conductivity, and electrical resistivity). The pair of second-order ordinary differential equations are solved numerically with constant temperature boundary conditions at both ends. The heat removal from the cathode base could be used instead of the base temperature depending on which parameter is known. The equation for the cylindrical portion is given by

$$0 = \frac{d^2\theta}{dZ^2} + \frac{I^2\rho_e L^2}{k_{th} T_{tip}\left[\pi (r_{cyl})^2\right]^2} - \frac{2\epsilon_r \sigma_r L^2 T_{tip}^3}{k_{th} r_{cyl}}\left[\theta^4 - \left(\frac{T_\infty}{T_{tip}}\right)^4\right] - \frac{2h_{conv} L^2}{k_{th} r_{cyl}}\left[\theta - \left(\frac{T_\infty}{T_{tip}}\right)\right] \quad (15)$$

for $Z_1 \leq Z \leq 1$ where $\theta = T/T_{tip}$, $Z = z/L$, and Z_1 is the axial location of the interface of the conical and the cylindrical portions. The equation for the conical portion is given by

$$0 = \frac{d^2\theta}{dZ^2} + \frac{2\tan\beta}{\cos\beta\,(Z\tan\beta + r_{cyl}/L)}\frac{d\theta}{dZ} + \frac{L^2\rho_e}{k_{th} T_{tip}[\pi(Z\tan\beta + r_{cyl}/L)]^2} - \frac{2\epsilon_r \sigma_r L T_{tip}^3}{\cos\beta\, k_{th}\,(Z\tan\beta + r_{cyl}/L)}\left[\theta^4 - \left(\frac{T_\infty}{T_{tip}}\right)^4\right] - \frac{2h_{conv} L}{\cos\beta\, k_{th}\,(Z\tan\beta + r_{cyl}/L)}\left[\theta - \left(\frac{T_\infty}{T_{tip}}\right)\right] \quad (16)$$

for $0 \leq Z \leq Z_1$. These second-order equations can be split into pairs of first-order equations using the transformation $Y_1 = \theta$ and $Y_2 = (d\theta/dZ)$. These sets of first-order equations for this boundary value problem are solved numerically using a shooting technique employing the fourth-order Runge-Kutta method coupled with the secant method. Note that the equations in both Refs. [10] and [19] contain errors; the correct relationships are given here by Eqns. 15 and 16.

Solutions for a cathode with a 12 mm diameter and 65 mm length are shown in Fig. (4) and Fig. (6) for a cylindrical geometry slid in Fig. (5) and Fig. (7) for the cylindrical cathode with a flattened conical tip shown in Fig. (3) ($r_{tip} = 2$ mm, and $\beta = 30°$). Figures 4 and 5 show the tip surface heat flux as a function of tip temperature with current as a parameter. Positive heat fluxes indicate that the plasma is heating the cathode, As the current is increased the allowable tip heat flux is reduced because of the increased Joule heating. Figures 6 and 7 show the axial temperature distributions within the cathodes for different current values. For these cases, only convective cooling is considered; that is, radiation is neglected and the base temperature is 1500 K. For the cylindrical geometry, the zero current case is the same as the pin-fin case previously considered. The allowable heat load to the cathode tip decreases with increasing current due to the heat generation from ohmic heating. For a given current value and tip temperature, the allowable tip heat flux is further decreased with the addition of a conical tip to the cathode. This is due to the decreased cross-sectional area and therefore the larger temperature gradient necessary for a given heat flux.

Figure 3: Illustration of a cylindrical cathode with a flattened conical tip.

The temperature distribution along the cathode is strongly dependent on the current value as seen in

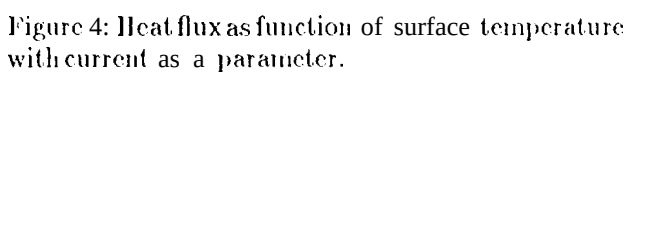

Figure 4: Heat flux as function of surface temperature with current as a parameter.

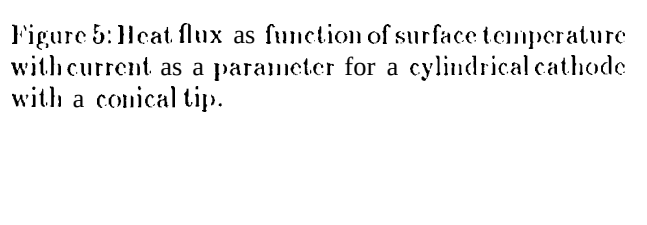

Figure 5: Heat flux as function of surface temperature with current as a parameter for a cylindrical cathode with a conical tip.

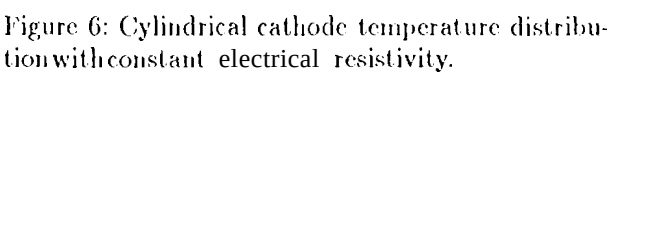

Figure 6: Cylindrical cathode temperature distribution with constant electrical resistivity.

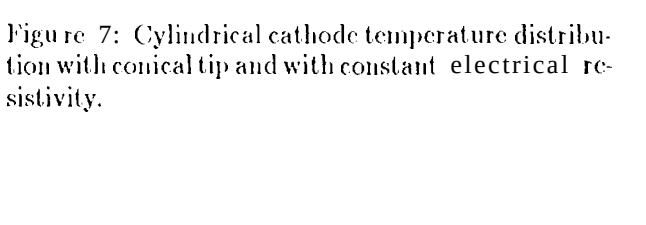

Figure 7: Cylindrical cathode temperature distribution with conical tip and with constant electrical resistivity.

figures 6 and 7. For large currents, the maximum temperature within the cathode is not at the tip but is towards the middle, which may explain the MPD thruster cathode melting observed at the University of Stuttgart [20]. This cathode apparently melted internally and ruptured due to excessive Joule heating leaving an external bulge and an internal hollow area[20]. The larger temperature gradients associated with the conical tip can also be seen.

One significant improvement to this model is the inclusion of temperature dependent electrical resistivity. While the thermal conductivity remains relatively constant, the electrical resistivity changes significantly over the range of temperatures expected for these cathodes, as seen in Fig. (8) [21].

Figure 8: Thermal conductivity and electrical resistivity for tungsten as a function of temperature.

A linear curve fit of the electrical resistivity provides the relation

$$\rho_e = (-12.457 + 0.0349T) \times 10^{-8} \qquad (17)$$

and a curve fit of the thermal conductivity data yields

$$k_{th} = 84.60 + 77.76 \exp\left(-7.995 \times 10^{-4} T\right) + 149.67 \exp\left(-5.026 \times 10^{-3} T\right) \qquad (18)$$

The linear resistivity can be substituted for the constant value of ρ_e in Eqns. 15 and 16. This change can significantly affect the results for currents greater than 1000 A, as seen by comparing Fig. (6) and Fig. (9).

Figure 9: Cylindrical cathode temperature distribution with temperature dependent electrical resistivity.

It is therefore important to use the temperature dependent properties for high-current cases, while the constant properties may be used for low-current cases. Using constant properties will simplify the numerical solution.

While these models are adequate for simple cathode geometries and boundary conditions (constant values) they are not sufficient to fully model the cathode characteristics in electric thrusters. It is expected that the plasma characteristics may change significantly along the cathode, and therefore the characteristics of the near-cathode plasma model will be significantly different. Also, observations at JPL have shown severe melting for conical-tip cathode and negligible melting with hemispherical-tip cathodes at similar and higher power levels [22]. A model capable of modeling a hemispherical-tipped cathode is also necessary.

One and One-Half-Dimensional Finite Difference Thermal Model

Experimental data suggest that for MPD thrusters the arc attachment may extend over a significant por-

tion of the exposed surface area [1]. Therefore, the thermal model must be capable of modeling ohmic heating and arc attachment over a range of axial positions as well as the tip. These cathodes can operate in either the tip attachment mode or a more diffuse attachment, illustrated in Fig. (10), depending on the discharge pressure.

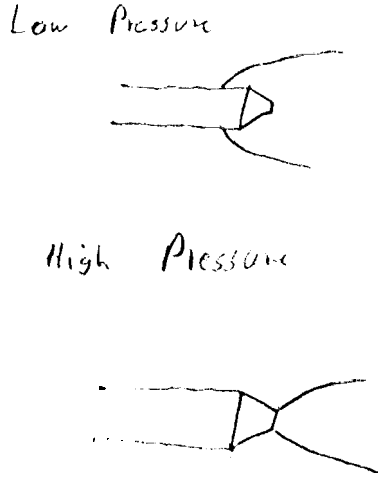

Figure 10: Illustration of high-pressure and low-pressure cathode arc attachment.

Temperature- dependent material properties are also required due to the large range of temperatures experienced in the cathode. For this study, a one and one-half-dimensional finite difference model (axial temperature distribution subject to radial boundary conditions) was developed. The model is capable of variable geometries, temperature-dependent material properties, and multimode heat transfer (arc attachment plus radiative and convective transport) at any axial location. The cathode is discretized axially into a given number of cells. The steady state heat equation,

$$\frac{d}{dx}\left(k_{th}A_C\frac{dT}{dx}\right) + \frac{dA_{surf}}{dx}q_{surf} + \dot{q}_{gen}\frac{dVol}{dx} = 0, \quad (19)$$

is solved using central finite differencing for each cell edge and the method of successive-over-relaxation to solve the global set of equations.

The total current is determined by integrating the current density values over the emitting surface. For conditions where the arc is attached over a major portion of the cathode surface, and therefore a large range of cathode temperatures exists, the surface heat flux can vary significantly. That is, because the cathode surface temperature will change significantly, so will the heat flux and the current density to the surface.

Combined Thermal and Plasma Model Solutions

The near-cathode plasma model and the cathode thermal model are combined to form an overall model of the cathode-plasma interaction. Figure (11) shows the heat flux and surface temperature relations for both the near-cathode plasma model and the simple heat transfer model (tungsten rod with a 1/8 inch diameter and a 65 mm length). Solutions exist at three points; namely, at the origin (trivial solution) and the two nonzero solutions where the curves intersect. Of these, only the high temperature (fully ionized) solution is numerically stable. Therefore, the value of the pressure is important for this type of discharge and the energy balance in the ionization region is not needed. The infinite fin solution is also shown in Fig. (11) for a convection coefficient of 5 W/cm^2/K and an environmental temperature of 500 K. Note

Figure 11: Heat flux as function of surface temperature with thermal model solutions.

that for operation where only tip attachment occurs, all combinations of the model parameters are not possible.

For the plasma conditions shown in Pig. (11) for the one-dimensional solution of Eq. (12), 420 W were applied at the cathode tip with a current of 502 A and a surface temperature of 2700 1{. At these conditions the ohmic heating would be about 100" W. Note that this effect is not included in either Eq. (12) or Eq. (13). For the infinite fin solution, the heat load is 1.0 kW with a current of 340 A and a tip temperature of 2620 K. For this case ohmic heating would be about 50 W. While Ohmic heating can be neglected for the conditions used for the infinite fin solution, it should not be neglected for the conditions used in the one-dimensional case where Ohmic heating is comparable to the heat flux from the plasma.

For the special case where the arc only attaches at the tip, such as for the arcjet, a series of solutions can be reasonably determined. For a given set of tllcrmal characteristics (h_{conv}, k_{th}, L, and A_C) for the one-dimensional model, and given the plasma properties, one can solve for the intercept point of the one-dimensional thermal model and near-cathode plasma model for the fully ionized (stable) case. The model parameters can then be adjusted to examine their effects on the solution. For example, consider the case of zero heat flux to the surface from the plasma. This special case does not depend on the type of thermal model or on the thermal model parameters, and therefore provides a good reference point for examining the plasma effects. Generally, for cases without internal heat generation (one-dimensional thermal model), the tip temperature solution will be bounded by the point of maximum heat flax (peak of curve) and the zero heat flux solution. This range of solutions can be limited for certain combinations of parameters, for example, small sheath voltages. That is, the difference between the zero heat-flux temperature and the peak temperature may be small. The limiting tip temperature solutions arc shown in Figs. 12 and 13 as a function of the sheath voltage. Note that two different sheath voltages can produce the same cathode tip temperature and that a temperature minimum exists. The decreasing temperature with decreasing voltage for the large voltage range is a result of decreasing ion energies. For small voltages, the plasma electron heating becomes significant and

Figure 12: Peak and zero point temperatures as a function of normalized sheath voltage with work function as a parameter

Figure 13: Peak and zero point temperatures as a function of normalized sheath voltage with pressure as a parameter.

dominates for very small voltages (< 4 volts). A minimum sheath voltage exists at the point where T_{peak} and T_{zero} are the same. This minimum is not the same as the minimum discussed previously although the voltage values for both may be similar. The tip temperature is strongly dependent 011 both the pressure and the material work function. Although a three orders of magnitude change in pressure for a specific thruster is not probable, it is not inconceivable for the material work function to change over the range of 1 eV shown.

Plots of attachment area as a function of sheath voltage can be seen in Fig. (14), and as a function of tip temperature in Fig. (15). The same dual solution

Figure 14: Arc attachment area as a function of normalized sheath voltage with work function as a parameter.

can be seen for attachment area as for temperature because the two arc related. As the sheath voltage drops from a high value, the cathode temperature decreases because the ion energy transferred to the surface is decreasing. The decrease in temperature produces a comparable decrease in thermionic current . Therefore the attachment area must increase to maintain the same total current since j_i and j_b are both decreasing. The minimum in temperature corresponds to the maximum in attachment area. As the voltage is further decreased the temperature begins to increase as the plasma electron heating becomes important. Even though the plasma electron current is

Figure 15: Arc attachment area as a function of cathode temperature with work function as a parameter.

increasing, the thermionic current is increasing faster and therefore the attachment area decreases. Figure 15 illustrates both solutions. For a given tip temperature, two attachment area values may be possible corresponding to two different sheath voltages. The smaller attachment area will have the larger sheath voltage. Also, for a given attachment area, two temperature solutions may be possible with the smaller temperature corresponding to the larger voltage. The actual thruster may operate in either the high-voltage mode or the low-voltage mode depending on the specific discharge characteristics [23]. It is also possible for the discharge to transition between these modes. The experiments may reveal which operational mode dominates for a given set of operating parameters.

Comparison with experiments

An example solution using the finite difference one and one-half dimensional thermal model is compared with experimental data in Fig. (16). For this example, the arc attachment was constrained to the region within 5 mm of the tip (hemispherical tip). The experimental temperature data were obtained from Ref. [24]. For this case, the current was 2255 A, ohmic heating produced 2.?1 kW, the arc heat load was 243 W, and the heats removed by radiation and cooling at the cathode base were 1.56 kW and 898 W

Figure 16: Temperature distributions in MPD thruster cathode.

respectively. Clearly, ohmic heating is the dominant heating source. The tip temperature was **3419 K.** It should be noted that the experimental current was fixed for only about 2 minutes at each condition. Therefore, the cathode was not in thermal equilibrium and the measured temperature profile may be off slightly. Additional experimental data are needed for cathodes in thermal equilibrium to verify the model. Also, the abrupt change in the experimental profile at a location of about 30 mm may be due to a change in the emissivity because of increased thorium coverage and is therefore not an actual temperature change [24]. This characteristic was observed at many different test conditions.

Conclusions

An overall model describing the operation of high current cathodes has been developed. The model combines a description of the near-cathode plasma with a thermal model of the cathode. For the high pressure discharges (about 1 atm) associated with arcjet thrusters where the primarily attaches a the cathode tip, a simpler one-dimensional thermal model can be used. For a given set of operating parameters, the overall model predicts a range of operating temperatures and arc attachments area.s for this type of discharge. Also, for a given set of operating conditions, it is possible to have two different cathode temperatures (with two different sheath voltages) for a given attachment area, or vice Versa. This indicates that there arc two operating modes for the arc attachment.

For low pressure disc. arges where the arc attachment is not confined to the tip region alone, a more complicated thermal model is required. This model must be capable of radial heat loads as well as axial ones. Preliminary model results indicate that for this type of operation, the temperature of the cathode in the arc attachment region is relatively constant. Experimental data from University of Stuttgart also shows this trend, indicating that the model is providing an adequate description of the cathode arc physics.

Acknowledgements

The research described in this paper was conducted at the Jet Propulsion Laboratory, California Institute of Technology, and was sponsored by National Aeronautics and Space Administration.

List of Variables with typical units

A	area (m^2)
A_R	Richardson coefficient ($A/m^2/K^2$)
d	cathode diameter (m)
e	electron charge (C)
E	electric field (V/m)
$E_{b,o}$	Normalized thermionic electron thermal energy
F	particle flux (particle/s)
h_{conv}	thermal convection coefficient ($W/m^2/K$)
I	total current (A)
j	current density (A/m^2)
J_b	normalized thermionic current density
k	Boltzman constant (J/K)
k_{th}	thermal conductivity (\V/in/K)
L	characteristic length (m)
m	particle mass (kg)
n	number density ($particle/m^3$)
P	pressure (l'a)
q	heat flux (W/m^2)
r	radius (m)
r_{cyl}	cylindrical radius (m)
R_c	radius of arc attachment spot (m)
$\dot{q}$	heat generated per unit volume (W/m^3)
T	temperature (K)
T_∞	environmental temperature (K)
v	velocity (111/s)
V	voltage (V)
Vol	volume (m^3)
x	position from cathode surface (m)
z	position from cathode tip (m)
Z	normalized position from cathode tip
Z_l	normalized position from cathode tip to conical base
α	ionization fraction
β	conical half-angle
ϵ	normalized electric field
ϵ_i	ionization energy (eV)
ϵ_o	permitivity of free space ($C^2/N/m^2$)
ϵ_r	emissivity
η	normalized voltage
η_i	normalized ionization energy

ν_i	normalized ion density at sheath edge
η_B	normalized Bohm energy
ρ_e	electrical resistivity (Ω - m)
ϕ	work function (eV)
σ_r	Stephen-Boltzmann constant ($W/m^2/K^4$)
θ	normalized temperature

subscripts

b	thermionic (beam) electron
base	cathode base
B	Bohm energy value
c	cathode surface
c	cross-sectional
D	Debye
e	plasma electron
eff	effective
ei	electron-ion collision
i	ion
n	neutral
p	main plasma
o	reference value
sh	sheath edge
surf	surface
tip	cathode tip
tot	total

References

[1] J. E. Polk, A. J. Kelly, and R. G. Jahn. Mechanisms of Hot Cathode Erosion in MPD Thrusters. In *21st International Electric Propulsion Conference*, Orlando, FL, 1990. AIAA-90-2673.

[2] K. Kuwahara, M. Morioka, S. Morimoto, S. Enya, and K. Kuriki. Thermal Characteristics of MPD Arcjet. In *17th International Electric Propulsion Conference*, Tokyo, Japan, 1984. IEPC 84-59.

[3] K. T. Shih, E. Pfender, W. E. Ibele, and E. R. G. Eckert. Experimental Studies of the Electrode Heat Transfer in a MPD Arc Configuration. In *Electric Propulsion and Plasmadynamics Conference*, Colorado Springs, CO, 1967. AIAA 67-673.

[4] P. D. Prewett and J. E. Allen. The Double Sheath Associated with a Hot Cathode. *Proceedings of the Royal Society of London*, 348:435-446, 1976.

[5] W. D. Deininger, A. Chopra, K. D. Goodfellow, and J. W. Barnett. Cathode Erosion Test for 30 kW Arcjets. In *25th Joint Propulsion Conference*, Monterey, CA, 1989. AIAA 89-2264.

[6] K. D. Goodfellow and S, N. B. Murthy. Electrode Processes and MPD Thruster Operation. In *24th Joint Propulsion Conference*, Boston, MA, 1988. AIAA-88-3207.

[7] D. E. Siegfried and P. J. Wilbur. A Model for Mercury Orificed Hollow Cathodes: Theory and Experiment. *AIAA Journal*, 22(10):1405-1412, 1984.

[8] A. Salhi and P. J. Turchi. A First-Principles Model for Orificed Hollow Cathode Operation. In *28th Joint Propulsion Conference*, Nashville, TN, 1992. AIAA 92.-3742.

[9] W. L. Bade and J. M. Yes. Arcjet Technology Research and Development-Final Report. Technical Report NASA CR-54687 and ItAIJ-65-37, Contract NAS 3-5900, AVCO Corporation, Wilmington MA, for NASA Lewis Research Center, Cleveland 011, 19G5.

[10] R. C. Mehta. Thermal Analysis of a Conical Cathode of an MPD Arc. *AIAA Journal*, 17(11):1272-1274, 1979.

[11] T. Weng and E. J. Seldin. Calculation of Steady State Temperatures in Graphite electrodes in an Electric Arc Steel Furnace. *Carbon*, 15:391-398, 1977.

[12] D. Q. King. Feasibility of Steady-State Multi-Megawatt MPD Thrusters. In *18th International Electric Propulsion Conference*, Alexandria, VA, 1985. AIAA 85-2004.

[13] K. D. Goodfellow, T. J. Pivirotto, and J. E. Polk. Applied-Field Magnetoplasmadynamic Engine Developments. In *28th Joint Propulsion Conference*, Nashville, TN, 1992. AIAA 92-3293.

[14] J. E. Polk. Operation of Thoriated Tungsten Cathodes. In **101}'** *Symposium, Space Nuclear Power Systems*, Albuquerque, NM, 1993.

[15] W. Neumann. *The Mechanism of the Thermoemitting Arc Cathode.* Akademie-Verlag Press, Berlin, Germany, 1987.

[16] D. Bohm. *The Characteristics of Electrical Discharges in Magnetic Plasma.* Mc Graw-Hill, New York, 1949.

[17] F. P. Incropera and D. P. DeWitt. *Fundamentals of Heat Transfer.* John Wiley and Sons, New York, 1981.

[18] J. E. Polk and K. 1). Goodfellow. High Current Cathode Thermal Behavior, Part 1: Experiments. In 23rd *International Electric Propulsion Conference*, Seattle, WA, 1993. IEPC 93-029.

[19] **1{. C.** Mehta. Transient Heat Transfer Analysis of a Conical Cathode of an MPD Arc. *AIAA Journal*, 24(2):346- 348, 1986.

[20] M. Auweter-Kurtz, B. Glocker, H. L. Kurtz, 0. Loesener, H. 0. Scharde, N. Tubanos, T. Wegmann, D. Willer, and J.E. Polk. Cathode Phenomena in Plasma Thrusters. In 21st *International Electric Propulsion Conference*, Orlando, FL, 1990. AIAA **90-2662.**

[21] editor R. C. Weast. *The Handbook of Chemistry and Physics, 65th ed.* CRC Press, Boca Raton, FL, 1984.

[22] **'J'. J.** Pivirotto and 1{. D. Goodfellow. An Experimental And Numerical Investigation of an Applied-Field Magnetoplasmadynamic Space Propulsion Engine. In 22nd *International Electric Propulsion Conference*, Viareggio, Italy, 1991. IEPC 91-074.

[23] J. F. Waymouth. Analysis of Cathode-Spot Behavior in High-Pressure Discharge Lamps. *Journal Light and Visual Enviroment*, 6(2):53 64, 1982.

[24] J. E. Polk. *Mechanisms of Cathode Erosion in Plasma Thrusters.* PhD thesis, Princeton University, Princeton, NJ, USA, to be published.

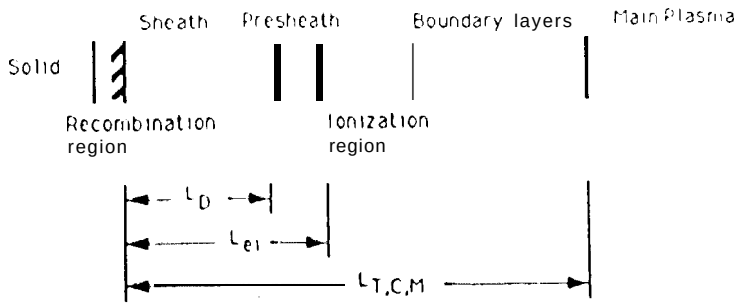

Fig 1

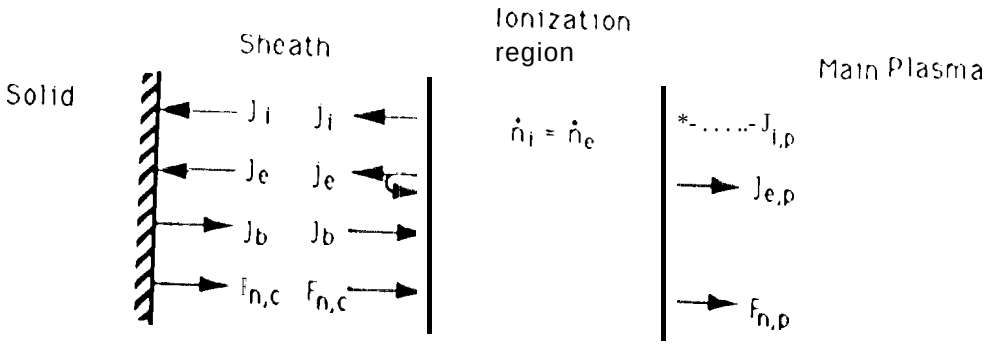

Figure 2: Illustration of Ionization Region

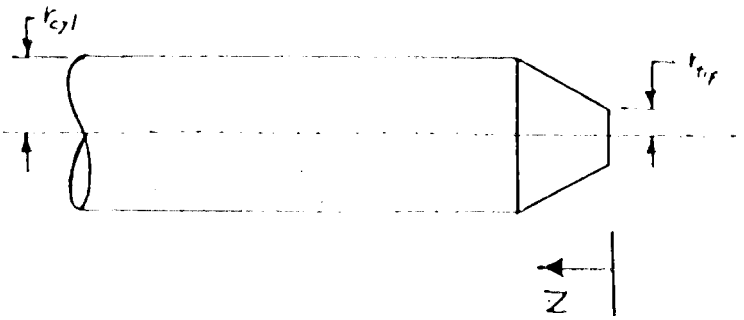

Figure 3: Illustration of a cylindrical cathode with a flattened conical tip.

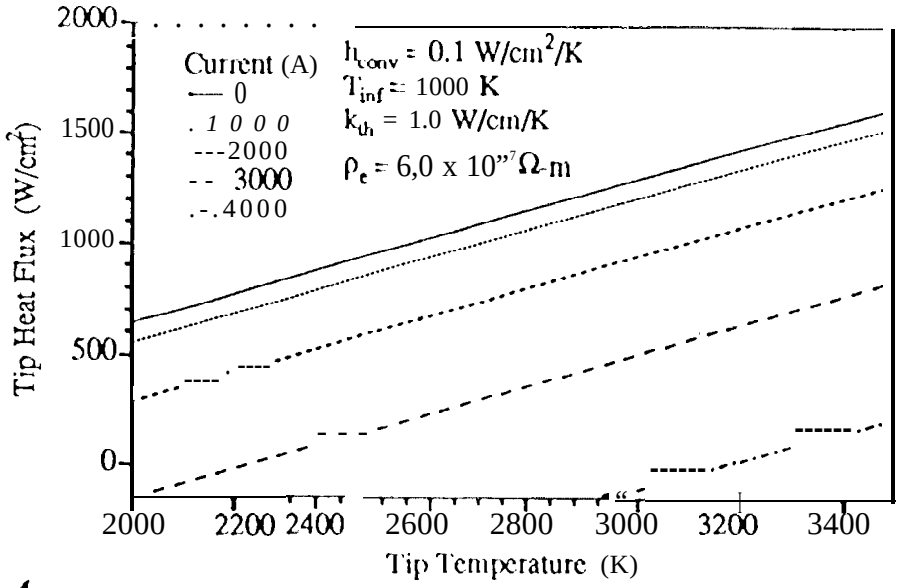

Figure 2.28: Heat flux as function of surface temperature with current as a parameter.

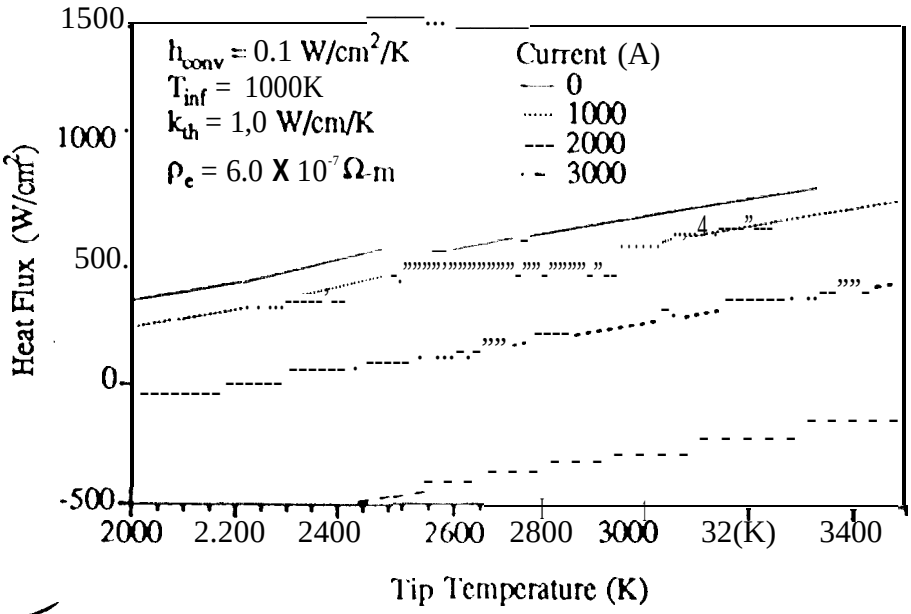

Figure 2.29: neat flux as function of surface temperature with current as a parameter for a cylindrical cathode with a conical tip.

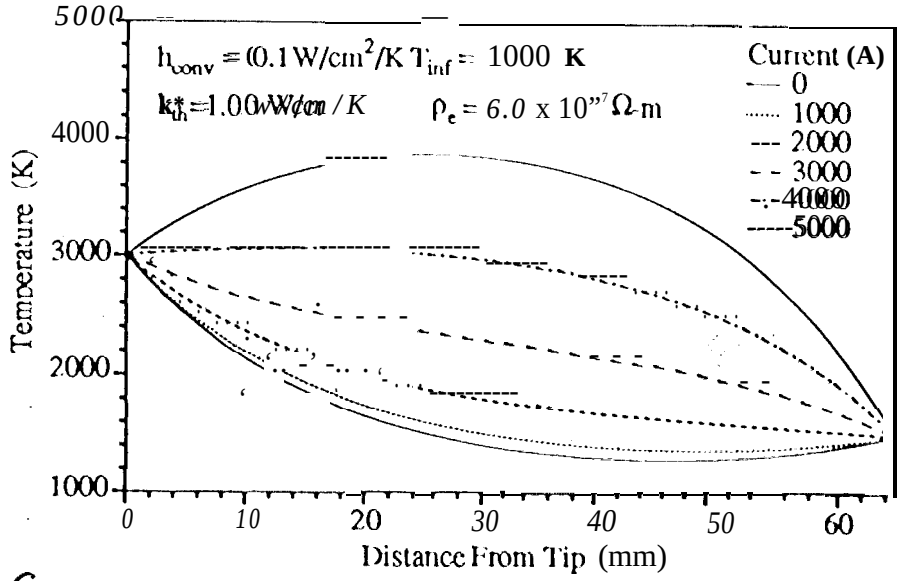

Figure 2.30: Cylindrical cathode temperature distribution with constant electrical resistivity.

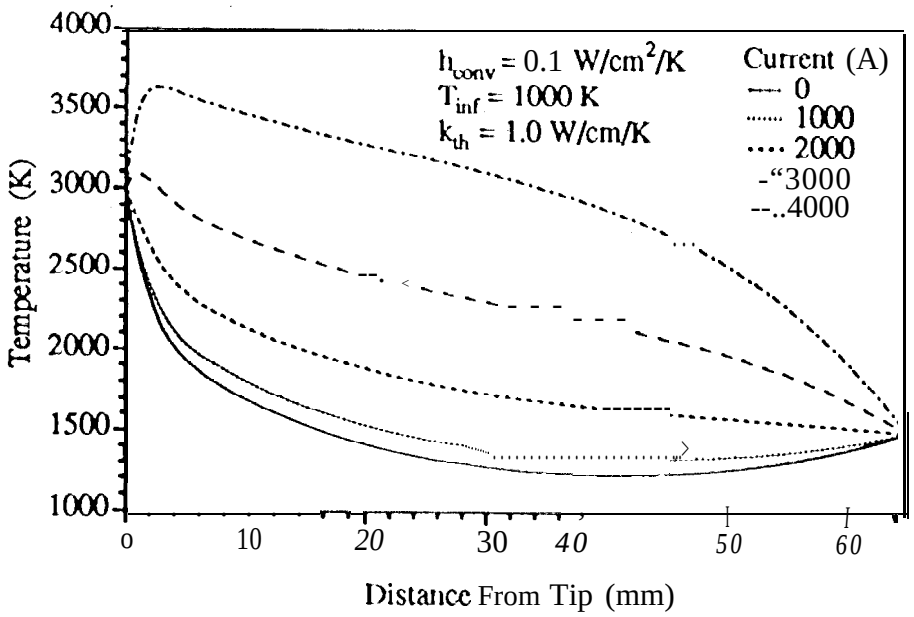

Figure 2.31: Cylindrical cathode temperature distribution with conical tip and with constant electrical resistivity.

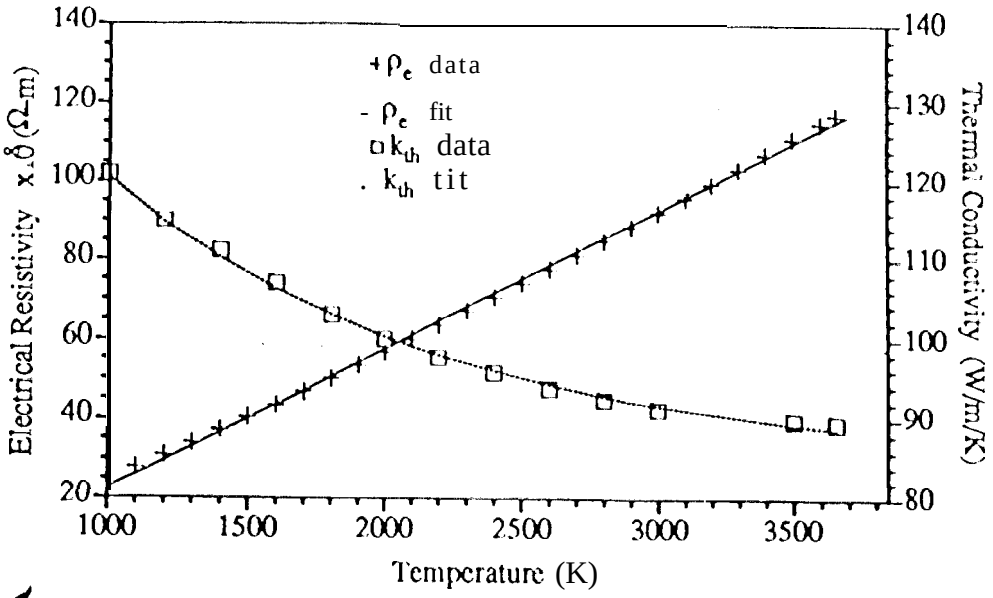

Figure 2.32: Thermal conductivity and electrical resistivity for tungsten as a function of temperature.

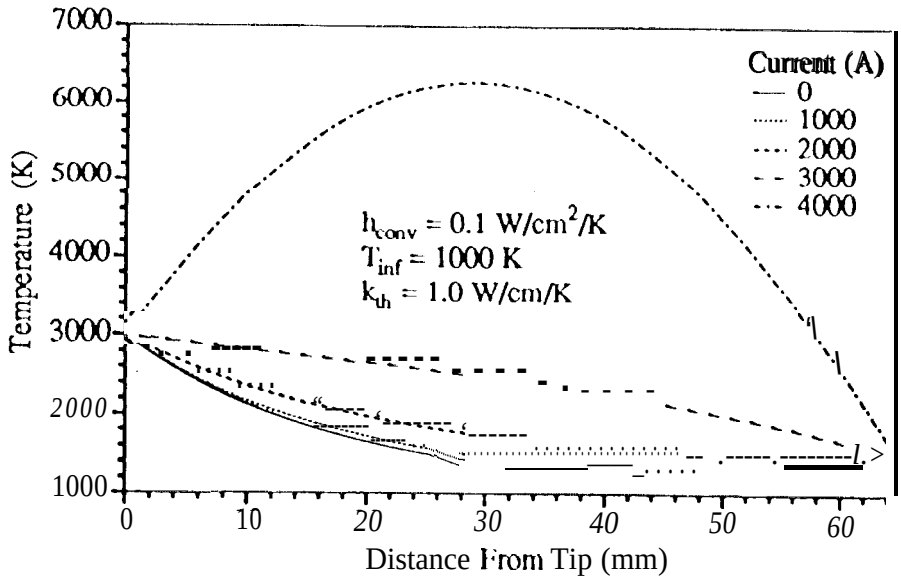

Figure 2.33: Cylindrical cathode temperature distribution with temperature dependent electrical resistivity.

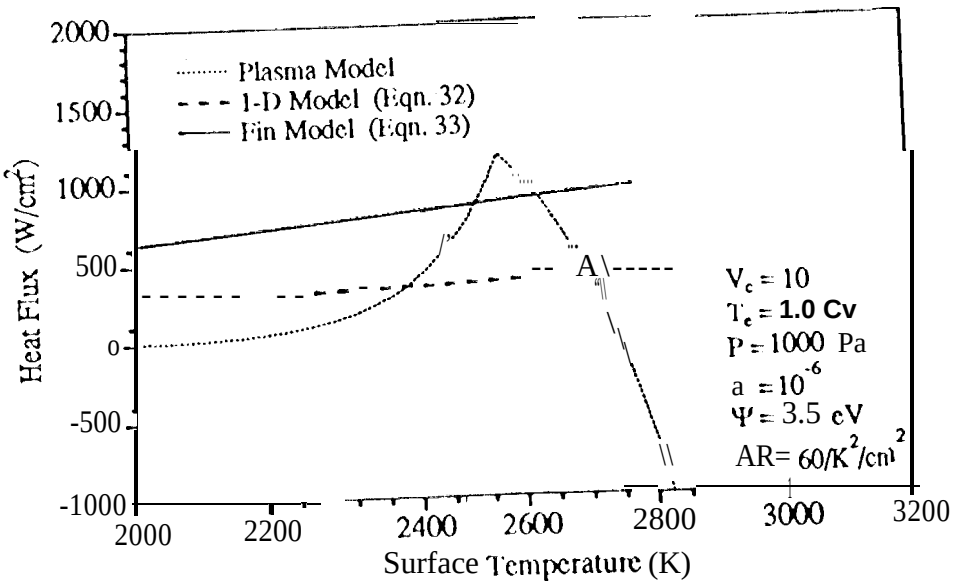

Figure 2.34: Heat flux as function of surface temperature with thermal model solutions

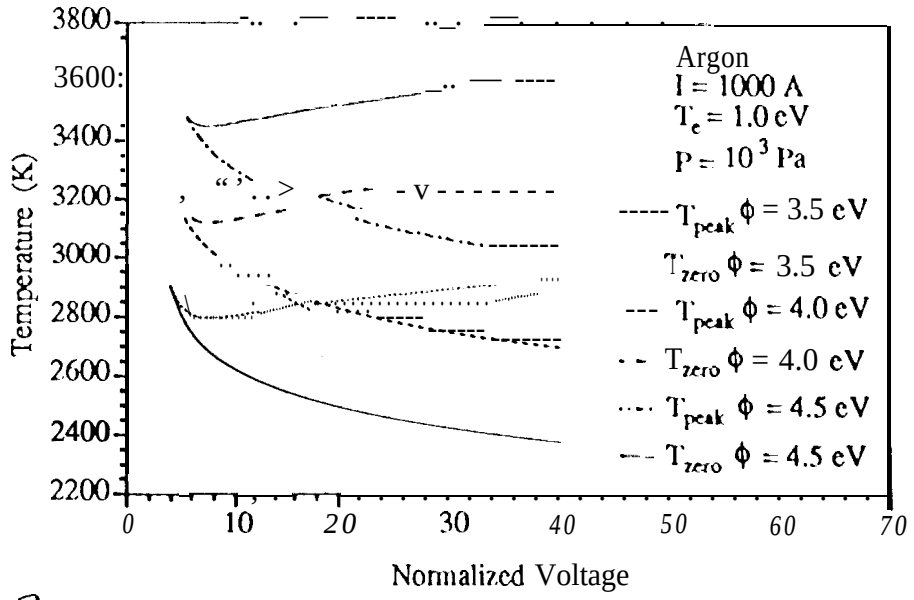

12

Figure 2.35: Peak and zero point temperatures as a function of normalized sheath voltage with work function as a parameter.

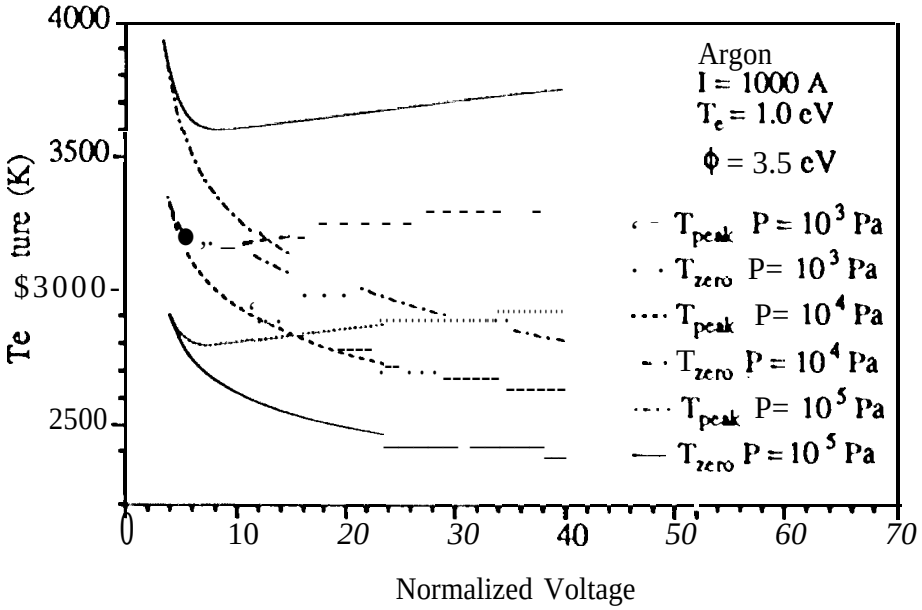

13

Figure 2.36: Peak and zero point temperatures as a function of normalized sheath voltage with pressure as a parameter.

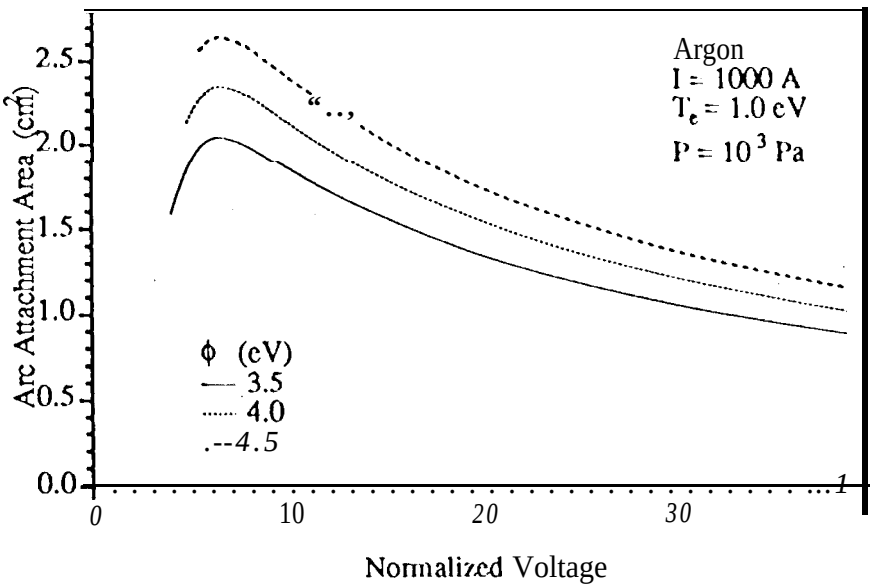

19

Figure 2.87: Arc attachment area as a function of normalized sheath voltage with work function as a parameter.

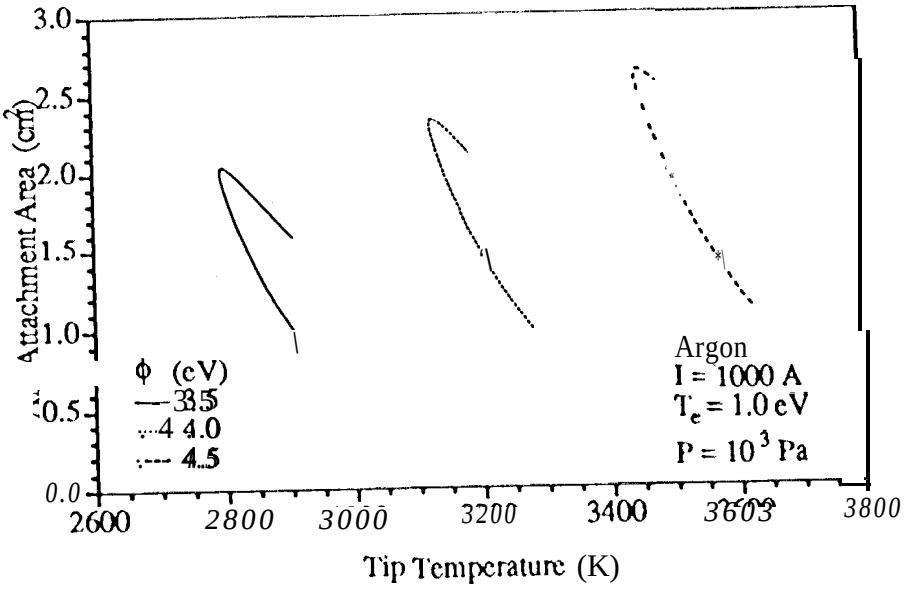

15

Figure 2.88: Arc attachment area as a function of cathode temperature with work function as a parameter.

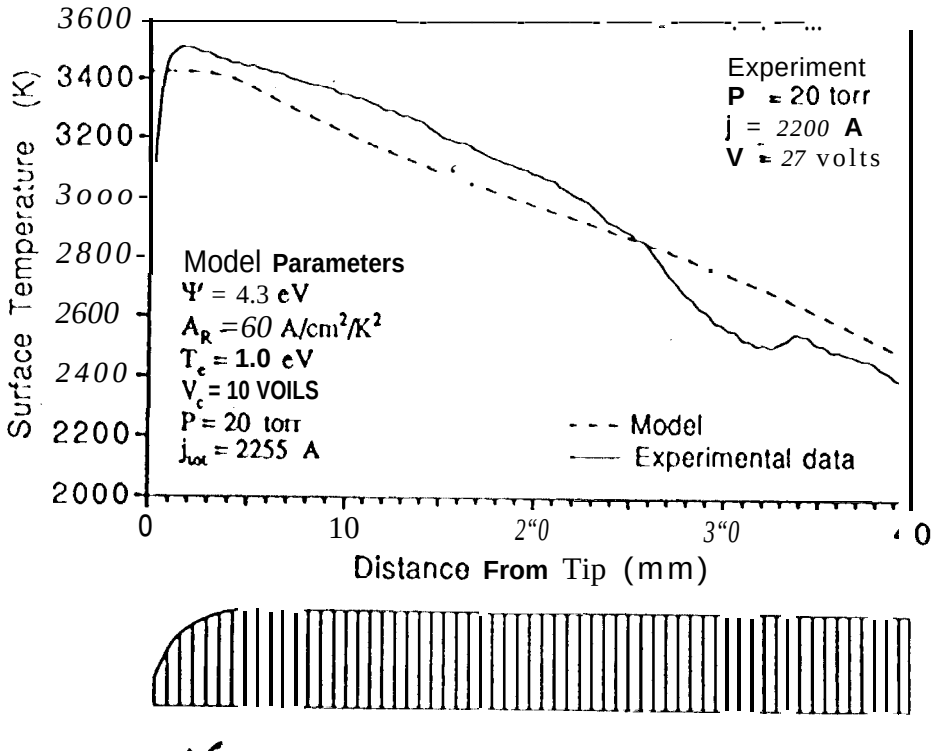

16

Figure 2.89: Temperature distributions in MPD thruster cathode,